Modulating Lamb waves with a tunable ultrasonic lens

Xiaowei Yin [a], Yanfeng Shen[*a,b], Xianggui Qin[c]
[a]University of Michigan-Shanghai Jiao Tong University Joint Institute, Shanghai Jiao Tong University, Shanghai, 200240, China; [b]Shanghai Key Laboratory for Digital Maintenance of Buildings and Infrastructure, Shanghai,200240, China; [c]China Aviation Industry Chengdu Aircraft Industry (Group) Co., Chengdu, 610091, China

ABSTRACT

This paper presents a tunable ultrasonic lens for the flexible control and modulation of Lamb waves. The lens is comprised of layered slice structures using Shape Memory Alloy (SMA) which could change its material properties under thermal loads. Numerical investigations on the wave dispersion characteristics demonstrate the tuning capability of wave speeds in the slice waveguide. Harmonic and transient dynamic modeling results further present the wave steering and focusing phenomena to a desired direction and focal point, covering a scanning area. Such a capability possesses great application potential to enhance the performance of Lamb wave based SHM and NDE systems.

Keywords: tunable surface structure, shape memory alloy, wave manipulation, wave front control, guided waves, ultrasonics

1. INTRODUCTION

Ultrasonic guided waves have been widely investigated as a powerful tool for structural health monitoring (SHM) and nondestructive evaluation (NDE) due to their outstanding ability to propagate long distances with little energy loss as well as their superb sensitivity to incipient structural changes. There's a growing interest in controlling the propagation of guided waves to achieve better performance in SHM and NDE via various types of engineered surface structures.

Pioneer studies on surface bonded structures have achieved promising progresses in controlling the propagation of guided waves in plates using elastic metamaterials (EMMs) [1-[2], thickness-direction-sliced metamaterials [3-[4], surface bonded slice lens [5-[6], and other types of structural designs. Yan et al. proposed an EMM flat surface lens by bonding a 2D planar array of pillar resonators on the host plate [1]. The unit cells in the array were made of two-layer composite stubs i.e., Pb disc deposited on a silicon rubber layer. Based on the working mechanism of EMM and the theory of geometrical optics, A0 Lamb waves focusing was realized. Later on, Zhu et al. introduced a perforated hexagonal microstructure unit cell in a stainless-steel plate to generate translational and rotational resonances simultaneously [2]. Through optimizing the geometrical parameters, a double-negative EMM plate with negative mass density and negative bulk modulus was realized. In addition, the negative refraction of longitudinal elastic waves at the deep-subwavelength scale was achieved. Thereafter, Su et al. modeled a solid metamaterial with aligned parallel gaps, with the solid material between these gaps playing the role of elastic waveguides [3]. Based on the wave bearing properties of the waveguides, focusing, refraction and asymmetric transmission of elastic waves were performed. Subsequently, an elastic metasurface was designed by cutting an array of aligned parallel cracks in a solid material [4]. As a result, the materials between the cracks could work as plate-like waveguides in the host medium. The array of waveguide with different thickness was capable of controlling the phase change of SV-waves while leaving the phase of P-waves unchanged. Thus, SV- and P-waves splitting was realized.

In 2017, Tian and Yu presented the simple surface bonded slice lenses to manipulate the propagation of Lamb waves through modulating the wavefront [5]. The lenses were made of metallic slices with designed shapes. It was numerically and experimentally demonstrated that a planer incident wavefront of A0 mode could be focused at a desired focal point with the proposed plano-concave aspherical lens. Their continuous research reported the elastic phased diffraction gratings for passive manipulation of ultrasonic guided waves in solid materials [6]. The effect of grating length on phase

[*]yanfeng.shen@sjtu.edu.cn; phone +86-21-34206765 Ext. 5021; fax +86-21-34206525

shift was theoretically proved. Besides, steering of plane waves, generation and manipulation of focused, pincer like, and curved guided wave beams were experimentally demonstrated by redesigning and changing the grating's superstrates.

These existing literatures demonstrated the successful control of guided waves via waveguide and surface designs. However, these research endeavors generally report wave manipulation designs which are not tunable, imposing considerable limitations on their practicable applications. Thus, the development of active and tunable wave control methodologies is drawing an increasing attention. Shape memory alloy (SMA) can change its mechanical properties under thermal loadings, which enables the design of active structural components for tunable wave control purpose.

SMA possesses two possible crystal phases, Martensite and Austenite [7]. SMA can exhibit unique thermal and mechanical behaviors, rendering a large deformation to recover an original shape or material modulus change. One of the most common and typical SMA material is Nitinol, which has found profound applications in medical devices and robotic systems as artificial muscles. The mechanism behind the shape memory effect stems from the phase transformation between the Martensite at low temperature and the Austenite at high temperature. Martensite phase is usually found at a lower temperature with a twinned configuration. After loading, the atomic structure becomes the de-twinned counterpart with retained strain in this phase. When temperature increases, Martensite phase would turn into Austenite, tracing back to its memorized shape status [8]. Pioneering investigations on applying SMA in active metamaterial designs have been carried out. They can generally be casted into two categories based on the mechanism of SMA. The first type of design utilizes the property of material elastic modulus change under thermal loadings [9]. Candido et al. proposed a metamaterial beam comprised of SMA resonators [11]. Its bandgap could achieve a significant shift with the change of temperature, and experiment results showed an obvious bandwidth increase. Another approach takes advantage of the large deformation ability of SMA. Chuang et al. proposed a flat-curved SMA resonator for realizing tunable bandgaps of a metamaterial beam [12]. It was reported that the curved resonator beam developed much lower-frequency and wider bandgaps, compared with the flat SMA resonator counterpart. In the same year, they developed another switchable EMMs beam by using similar bending SMA resonators that could transform back and forth between two statuses [13]. By exerting thermal loading on the unit cells, Bragg scattering and local resonance bandgaps could be switched, achieving an increasing tunable bandgap capability. It should be noted that current literatures on SMA metamaterials generally focus on the control of low-frequency vibrations. However, to the best of the authors' knowledge, wave manipulation using SMA has seldom been reported.

In this study, a new method is presented for realizing tunable Lamb wave control. This approach utilizes composite bonded waveguide slices of SMA via the elastic modulus change property. Arbitrary intermediate phasic states can be achieved by suitably controlling the temperature of the heating patches. Systematic numerical case studies and parametric designs are presented to demonstrate the capability of this acoustic lens for wave control and modulation.

2. DISPERSION CHARACTERISTICS OF COMPOSITE SLICE WAVEGUIDE UNITS

Figure 1 presents the proposed slice waveguide unit structure. It was comprised of two material layers with carefully designed shapes. The bottom layer was made of aluminum while the upper layer was made of SMA. The width of the composite slice was set as 2 *mm*. The thickness of each layer was tailored as 1.5 *mm*, with the length gauged as 30 *mm*. In order to increase the wave energy transmission, ramp-shape transition regions were added at both sides of the aluminum layer. This would ensure that more energy can propagate through the composite slice. The slice waveguide can change the local effective stiffness of host plate.

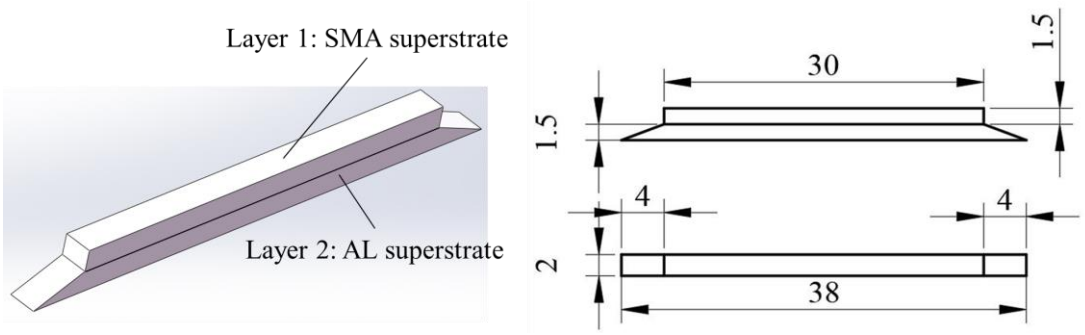

Figure 1 Structure of the proposed composite slice waveguide unit and its dimensional drawing.

Connected with heating patches, the elastic modulus of SMA can be properly modified to control the phase velocity of guided waves propagating through it. As a consequence, the wavefront could be controlled via the phase modulation in an array of waveguide slices. It will be demonstrated that a straight-crested A0 wavefront can be focused on a desired focal point with properly-distributed elastic modulus of the SMA. In addition, Lamb waves can be directed towards a certain direction by changing the elastic modulus of SMA through thermal loads.

In order to study the influence of elastic modulus change on wave velocity in the waveguide units, a Finite Element Model (FEM) of the slice cross section was built. An extra area was added as host plate connected to the slice waveguide, as shown in Figure 2(a). The Bloch-Floquet Boundary condition was implemented on the cross-sectional areas along the wave propagation direction. The elastic modulus of SMA superstrate elements was set as 30 GPa and 70 GPa in two case studies. The resultant dispersion curves is illustrated in Figure 2(b). Obvious changes could be observed. These results conveyed that the dispersive character of the composite slice waveguide is closely related to the elastic modulus of the SMA superstrate. In the subsequent case studies, the elastic modulus of the SMA superstrate was modeled for 35 GPa, 40 GPa, 45 GPa, 50 GPa, 55 GPa, 60 GPa, and 65 GPa, respectively. A0 Lamb mode velocities collected from these FEM simulations at 150 kHz are plotted in Figure 2(c). The polynomial-fitting of these data, long with the illustrations in references 9-10, may clearly demonstrate that by properly controlling the temperature of the heating patches on SMA, wave speeds could be accurately adjusted. This implies that forming a desired wavefront is possible.

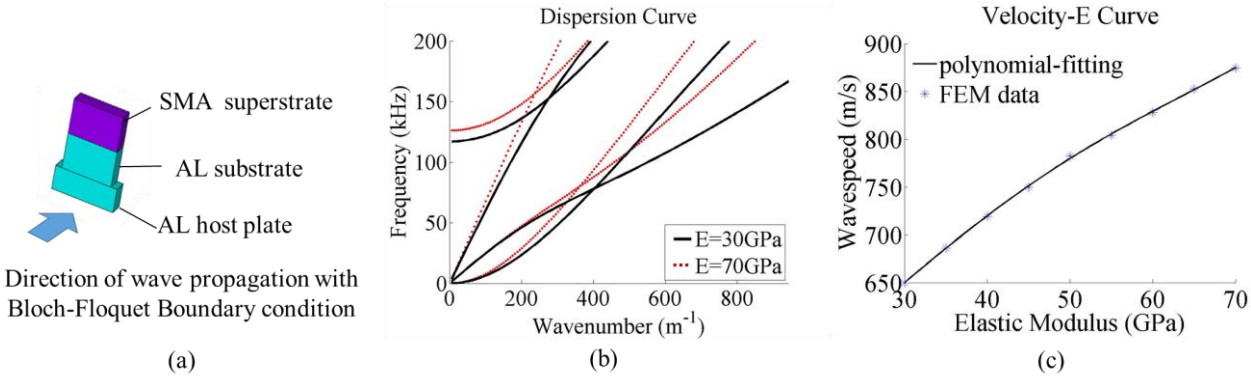

Figure 2. Numerical investigation of wave speed and material modulus relationship: (a) FEM for a cross-sectional area of the waveguide unit; (b) dispersion relation of the slice with different SMA elastic moduli: E = 30 GPa (black solid line) and E = 70 GPa (red dotted line); (c) velocity data and the polynomial-fitting of c-E relationship at f = 150 kHz.

3. LENS DESIGN, PRINCIPLE OF WAVE FOCUSING, DEVIATION, AND WAVEFRONT MODULATION

Focusing Lamb waves into a narrow beam possesses great application potential in the field of SHM and NDE [5, [14]. Compared with planer wave naturally generated by ultrasonic transducers, the focused waves forming a narrower beam with higher energy would provide a better spatial monitoring resolution and a higher signal-to-noise ratio for improved damage detection. In this section, a tunable ultrasonic lens is designed for focusing Lamb waves.

In geometrical optics, the plano-convex and plano-concave aspherical lenses can focus and expand light beams through refraction, respectively. The principle of these optical phenomena can be explained as the following: the spherical optical lens has a specific radius of curvature, and the velocity in the lens is varying at different thickness locations. Therefore, a focusing or expanding wavefront can be formed. Based on this working mechanism, researchers have proposed an elastic metasurface consisting of a rectangular-shape arranged array. Wave focusing was realized based on the unit cells with different elastic moduli and effective mass densities [1]. This approach simplified the shape design procedure of ultrasonic lenses to some degree. Inspired by such a principle, a tunable rectangular-shaped ultrasonic lens is proposed in this study. The research target is directed at focusing and deviating Lamb waves in a host plate through wavefront modulation.

As presented in Figure (a), the lens was made of 15 composite waveguide slices as proposed in the previous sections. The size of the lens was amounted to 38 *mm* along X-axis and 44 *mm* along Y-axis, with the interval between two slices occupying a 1-*mm* wide space. The aggregation of 15 slices would satisfy the requirement of gradually increasing the

elastic modulus distribution. In such a way, it can improve the continuity of wavefront modulation when the waves are propagating through the lens. The definition of directions is also depicted by the coordinate axis in Figure (a), where the Y+ direction and Y- direction are clearly marked out. These directions will be employed in the following discussions. In this structure, each waveguide slice is assumed to be ideally bonded on the host plate. Thus, the wave velocity distribution along Y-axis can be controlled as the red curves profiles in Figure (b-c) for realizing wave focusing and deviation, respectively.

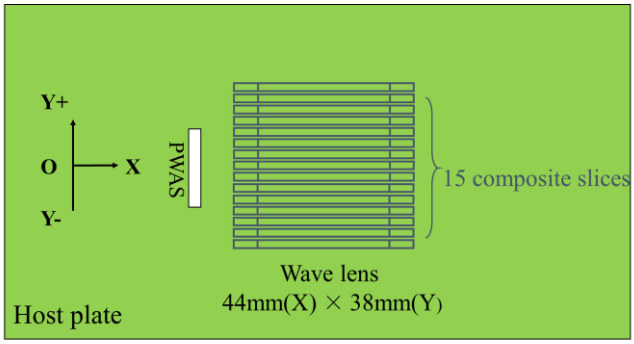

(a)

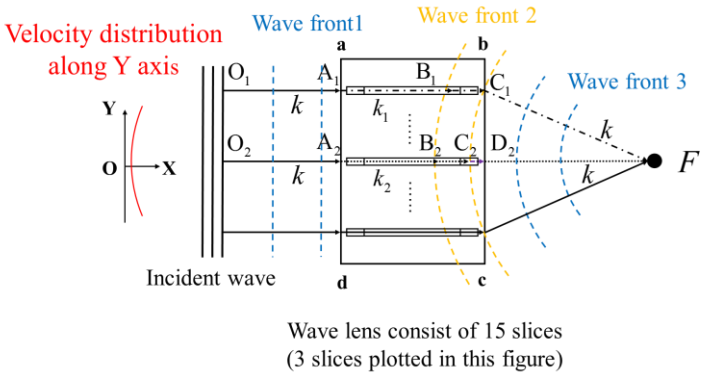

(b)

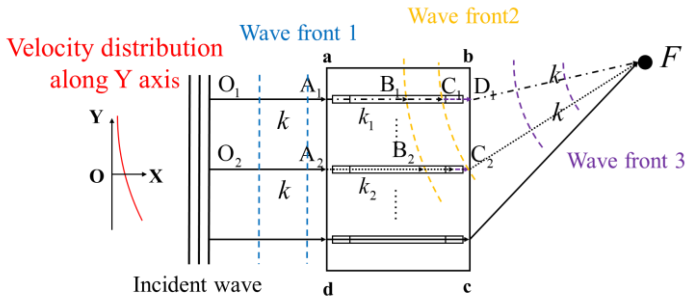

(c)

Figure 3. (a) Schematic of the rectangular-shaped ultrasonic wave lens with 15 composite slices; (b) principle of focusing Lamb waves using the rectangular-shaped lens; (c) principle of deviating Lamb waves using the rectangular-shaped lens.

It is assumed that the straight-crested incident Lamb waves propagate towards X+ direction in the plate with planar wavefronts parallel to the left edge of the wave lens, as indicated by wavefront 1 in Figure (b). In this case study, the waves entering the lens from the left edge **a-d** and exiting from the right-edge **b-c** are under consideration. In order to focus the incident waves on the focal point (*F*), the waves travelling along different paths (e.g., waves generated at points O_1 and O_2 marked in Figure (b)) should arrive at the focal point at the same time. In other words, the propagation time

along two different paths (as shown by $O_1A_1C_1F$ and $O_2A_2C_2D_2F$ in Figure (b)) from the wave source to the focal point should be the same:

$$\frac{O_1A_1}{c}+\frac{A_1C_1}{c_1}+\frac{C_1F}{c}=\frac{O_2A_2}{c}+\frac{A_2C_2}{c_2}+\frac{C_2D_2}{c_2}+\frac{D_2F}{c} \tag{1}$$

where c denotes the phase velocity in the host plate, c_1 and c_2 are the phase velocities in the composite slices following the velocity distribution, respectively. Substituting $c = \omega/k$, $c_1 = \omega/k_1$, and $c_2 = \omega/k_2$ into Equation (1) with k, and k_1 and k_2 being the wavenumbers in the host plate. In composite slice 1 and composite slice 2, Equation (1) can be rewritten as:

$$kO_1A_1+k_1A_1C_1+kC_1F=kO_2A_2+k_2A_2D_2+kD_2F \tag{2}$$

where $A_1C_1+C_1D_1=A_1D_1$. Equation (2) presents a pervasive expression of the relationship between wavenumbers and geometric parameters. On the basis of this expression, the rectangular lens can be designed to focus incoming planar Lamb waves on a desired focal point. The dispersion characters of the composite waveguide slices are utilized in the design procedure.

Thereafter, the wave propagating inside the lens are under consideration. Since c_1 is larger than c_2, wave 1 runs faster than wave 2. When wave 1 arrives at the right edge (i.e., point C_1), wave 2 arrives at point C_2, with a distance of C_2D_2 left behind. By properly setting the elastic modulus of the SMA layer bonded on each composite slice, a focusing phase velocity distribution can be achieved. Later on, when all the waves propagate out of the lens, the focusing wavefront is manipulated as series of concentric circles.

Based on this principle, if the elastic modulus increases monotonically along Y- direction, the incident wave can be deviated towards a certain direction, as shown in Figure (c). For explanation, the planar incident wave entering the left edge **a-d** and exiting from the right-edge **b-c** are taken into account. In order to focus the incident waves at the deviated focal point (*F*), the waves coming from different locations in the wavefront (e.g., O_1 and O_2 given in Figure (c)) would arrive at the deviated focal point at the same time. That is to say, the propagation time along two different paths (as shown by $O_1A_1C_1D_1F$ and $O_2A_2C_2F$ in Figure (c)) from the wave source to the focal point should be the same:

$$\frac{O_1A_1}{c}+\frac{A_1C_1}{c_1}+\frac{C_1D_1}{c_1}+\frac{D_1F}{c}=\frac{O_2A_2}{c}+\frac{A_2C_2}{c_2}+\frac{C_2F}{c} \tag{3}$$

Similar with the discussion on the first focusing case, Eq. (3) can be casted into the wavenumber expressions:

$$kO_1A_1+k_1A_1D_1+kD_1F=kO_2A_2+k_2A_2C_2+kC_2F \tag{4}$$

where $A_1D_1=A_1C_1+C_1D_1$. Equation (4) indicates a general formula of the relationship between wavenumbers and geometric parameters. Based on this equation and similar principle as illustrated in the previous case, the rectangular-shaped lens can deviate the incident planar Lamb waves to a desired direction and converge at a point (*F*).

In Figure , three propagation paths are plotted to describe the entire procedure of wave propagation. At first, the wavefront of the incident wave is straight. After passing through the lens, the velocity distribution was artificially controlled. As a result, the initially planar wavefront gradually turned into a focusing or deviation arc. Therefore, on the basis of wavefront manipulation, the wave can be steered in a desired direction.

4. NUMERCIAL CASE STUDIES FOR LAMB WAVE MODULATION DEMONSTRATION

Based on the principles discussed in the previous sections, a system of the tunable wave lens is constructed. The dynamic properties and wave manipulation ability of the wave lens are systematically investigated in this the section.

4.1 Spectral response of wave lens for wave focusing

An FEM of the tunable wave lens with 15 uniform surface-bonded waveguide slices was built to analyze its wave focusing performance. The distribution of elastic modulus in the waveguide slices is depicted in Figure (a). The elastic

modulus of the middle slice (i.e., slice 0) was set the smallest, and that of slice 7 and slice -7 shared the largest value. The schematic of the FEM is shown in Figure (b), with non-reflective boundaries added to the edge of the host plate. At the origin of X-axis, a line force loading was exerted for the harmonic analysis.

In the simulation, the sweeping frequency ranged from 50 kHz to 200 kHz. The host plate with a tunable wave lens was modeled first. Then, a comparative study of a pristine host plate without the lens was also conducted. In this way, the energy transmission ability of the proposed wave lens could be evaluated. A sensing point located 100 *mm* away from the loading location was selected for data collection.

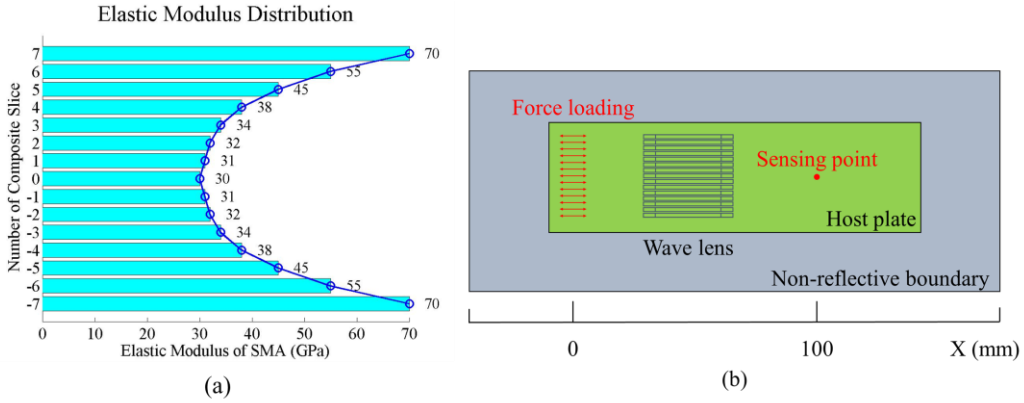

Figure 4. (a) Elastic modulus distribution in the wave focusing case; (b) schematic of the finite element model for studying the spectral response of the wave lens.

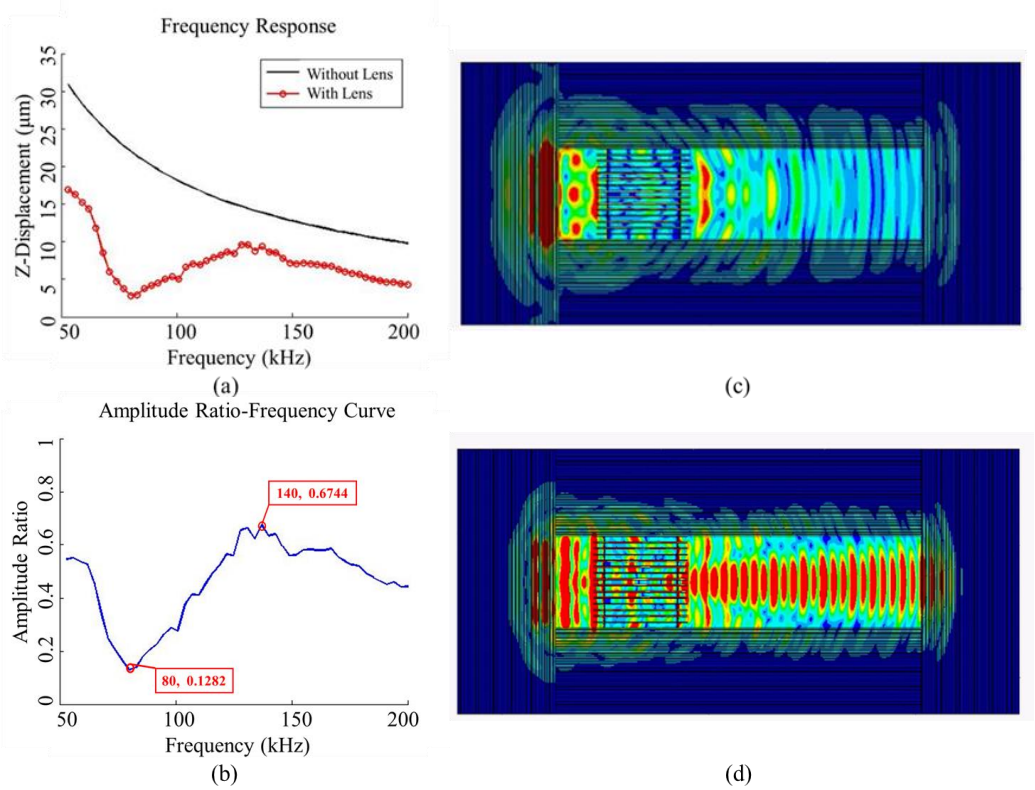

Figure 5. Harmonic response of the system with symmetric elastic modulus distribution: (a) harmonic response of host plates with and without the wave lens at the sensing location; (b) wave transmission coefficient evaluated at the sensing location; (c) harmonic response of the wave lens at f = 80 kHz; (d) harmonic response of the wave lens at f = 140 kHz.

The harmonic response of the sensing point is shown in Figure (a). The black line represents the pristine case, where the host structure was built without the wave lens. The red circled line illustrates the harmonic response of sensing point on the host structure with the wave lens. In order to further study the focusing ability of this system, the amplitude ratio $T = A_L / A_{NL}$ was defined as a general transmission coefficient. In this equation, A_L denoted the harmonic response of sensing point with the lens, and A_{NL} denoted the harmonic response of sensing point without the lens. The curve of amplitude ratio with respect to frequency is plotted in Figure (b). It could be observed that when the frequency reached 80 kHz, the wave transmission was relatively weak. Meanwhile, the harmonic response reached a peak value at 140 kHz.

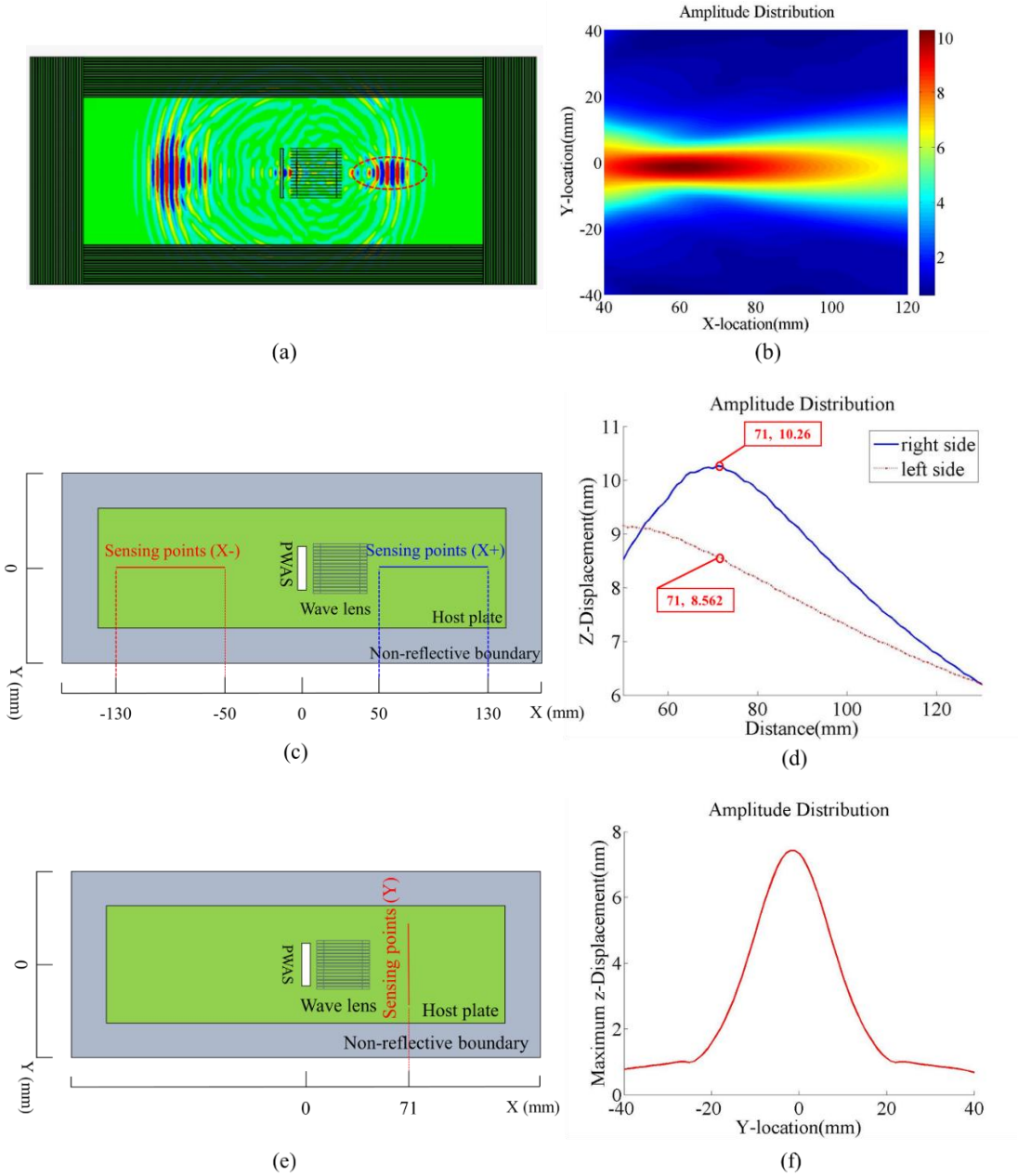

Figure 6. Transient dynamic response of the wave lens system: (a) particle velocity wave field of the system at t = 0.5 μs; (b) amplitude distribution of the focused wave energy on the right side of the wave lens; (c) schematic displaying the location of sensing points along X direction on both sides of the PWAS transducer; (d) wave amplitude distribution at the sensing points along X direction; (e) schematic displaying the location of sensing points along Y direction; (f) wave amplitude distribution at the sensing points along Y direction.

The corresponding equivalent strain distributions on the host structure are respectively displayed in Figure (c) and Figure (d), giving a more intuitive perception. These results indicated that 140 kHz was the best working frequency for the wave lens employing the elastic modulus distribution illustrated in Figure (a).

4.2 Temporal response of the wave lens system

After investigating the harmonic response of the lens system, its transient behavior was further studied, as illustrated in Figure (a). A 5-count, Hanning window modulated tone burst signal centered at 140 kHz was generated by the PWAS transducer. The particle velocity wave field at $t = 0.5\ \mu s$ illustrates that the generated wave underwent an obvious focus after exiting the wave lens. The energy distribution of the focused wave formed a narrow beam, as presented in Figure (b). In order to study the spatial feature of the planar and the focused wave fields and to determine the position of focal point, sensing points along X-axis were employed. These sensing points located symmetrically about the PWAS transducer, as plotted by the red line and the blue line in Figure (c). The lengths of both lines were set as 80 *mm*. Figure (d) displays the dynamic response amplitudes along these sensing points. The peak of wave amplitude was found at 71 *mm*, demonstrating the position of the focal point. Compared with the amplitudes of the sensing points on the left side, the amplitude of the focused wave was about 20% larger than that of the planar wave. Then, the amplitude distribution along Y-axis, ranging from -40 *mm* to 40 *mm*,was studied. Figure (e) demonstrates the amplitude was symmetrically distributed about the central line, with most of the wave energy focused at the center. These results exhibited the outstanding wave focusing ability of the proposed acoustic lens.

4.3 Wave focusing and deviation control by modifying the modulus distribution

In the previous section, obvious focusing has been realized by the ultrasonic wave lens. Based on this result, the modification of elastic modulus distribution is further conducted. Its influence on the wave steering capability will be illustrated in this section.

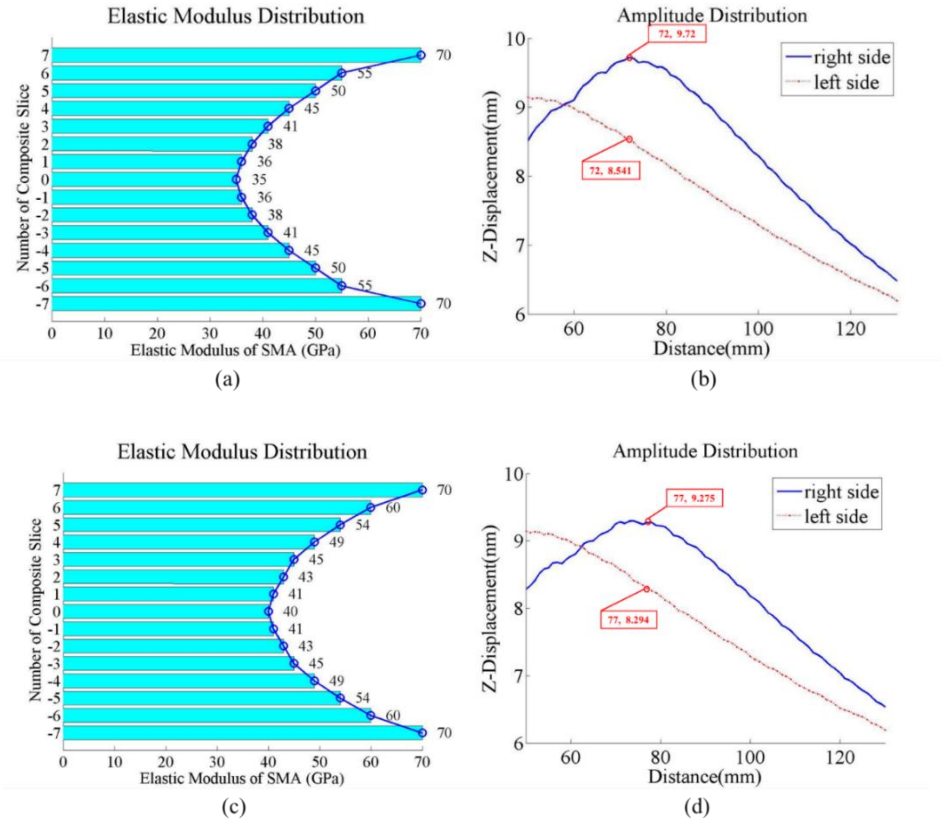

Figure 7. (a) Elastic modulus distribution of the 1st modified focusing lens slices; (b) resultant amplitude distribution on both sides of the PWAS; (c) elastic modulus distribution of the 2nd modified focusing lens slices; (d) resultant amplitude distribution on both sides of the PWAS.

The wave focusing distance adjustment will be demonstrated first. The details of the reconfigured values are shown in Figure (a). In this case, the smallest elastic modulus was elevated to 35 GPa at slice 0, 5 GPa larger than that in the previous section. Meanwhile, the largest value remained as 70 GPa. The corresponding wave amplitudes of sensing points on both sides are plotted in Figure (b). It could be observed that the location of the focal point moved 1 *mm* forward along X+ direction compared to the case in previous section. Then, the elastic modulus distribution was changed furthermore, as presented in Figure (c). The smallest elastic modulus increased to 40 GPa at slice 0, 10 GPa larger than that in the previous section. Meanwhile, the largest value remained as 70 GPa. The location of focal point moved 7 *mm* forward compared with the original case, as shown in Figure (d). These results demonstrated that the wave lens had the capability of focusing planar wave to different focal distance as wanted.

Finally, the elastic modulus distribution of SMA was modified as monotonical decrement long Y+ direction and increment along Y+ direction respectively, as illustrated in Figure (a) and Figure (c). The amplitude distribution obviously demonstrated that after exiting the acoustic lens, the incident waves were steered towards Y+ direction and Y- direction with a 6.25 ° deviation angle, respectively. Thus, the wave deviation capability of the proposed wave lens has been demonstrated.

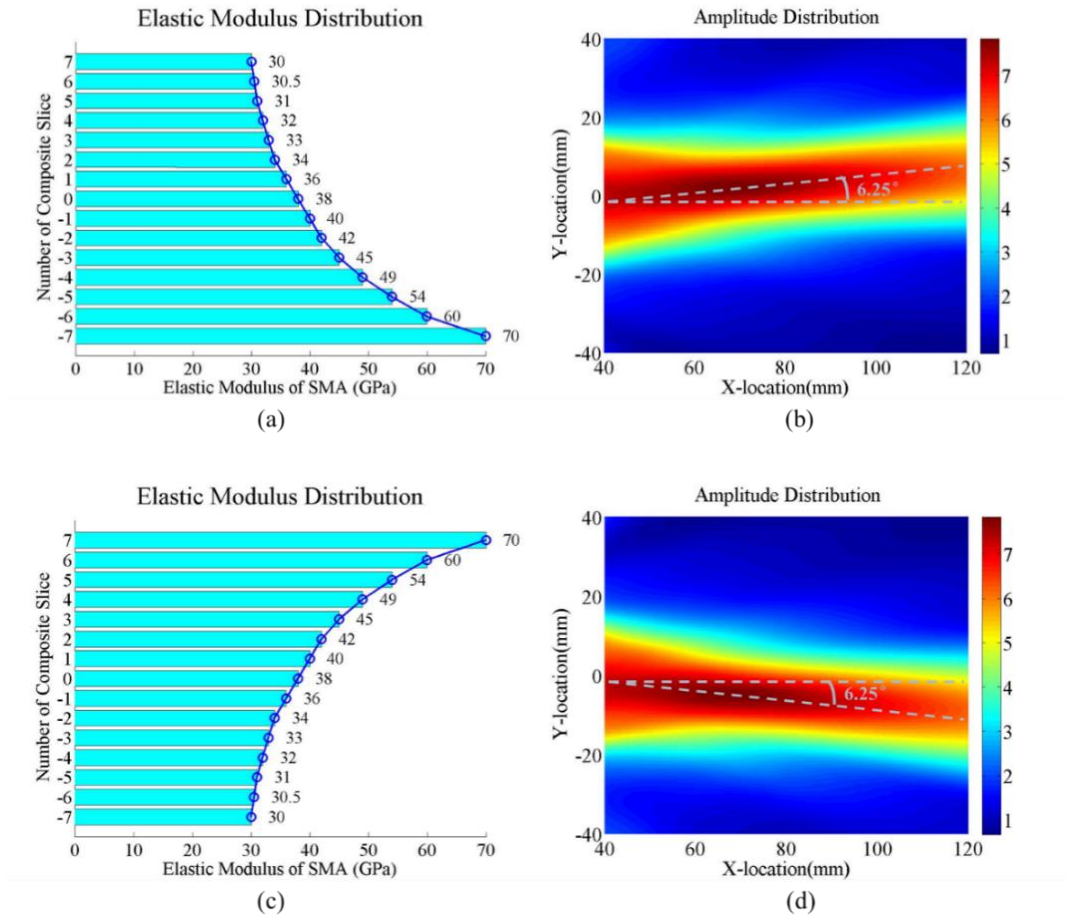

Figure 8. (a) Monotonically decreasing elastic modulus distribution along Y+ direction; (b) amplitude distribution of the upward deviated wave field on the right side of the wave lens; (c) monotonically increasing elastic modulus distribution along Y+ direction; (d) amplitude distribution of downward deviated wave field on the right side of the wave lens.

5. CONCLUDING REMARKS

In this study, a rectangular wave lens was presented for tunably controlling Lamb wave propagation. It could achieve wave focusing and deviation via the application of thermal loads. The composite waveguide slice structure is comprised of two material layers with carefully designed shapes, with the bottom layer made of aluminum while the upper layer made of SMA. The elastic modulus of SMA layers can be properly modified, so as to control the phase velocity of guided waves propagating through it. As a consequence, the focused and deviated wave front can be achieved via the phase modulation.

In order to design the composite waveguide slice and demonstrate the wave manipulating capability, the dispersion relationship was calculated for the slice with different values of elastic modulus. The results showed a considerable phase velocity increase with larger elastic modulus, which proved the tunable property of dispersive characteristics. The principle of wave focusing and deviation via the rectangular shape lens was demonstrated. Finite element simulations of the wave lens were conducted. The harmonic analysis facilitated the identification of sweet working frequencies. Finally, the wave steering capability of the system was demonstrated. The system presented outstanding performance in steering and focusing Lamb waves to a desired direction and focal point, enabling the coverage of a scanning area. Such a capability possesses great application potential to enhance the performance of Lamb wave-based SHM and NDE systems.

ACKNOWLEDGEMENTS

The support from the National Natural Science Foundation of China (contact number 51605284 & 51975357) is thankfully acknowledged.

REFERENCES

[1] Yan, X., Zhu, R., Huang, G., & Yuan, F. G., "Focusing guided waves using surface bonded elastic metamaterials," Applied Physics Letters, 103(12), 121901-121905 (2013).
[2] Zhu, R., Liu, X. N., Hu, G. K., Sun, C. T., & Huang, G. L., "Negative refraction of elastic waves at the deep-subwavelength scale in a single-phase metamaterial," Nature Communications, 5, 5510 (2014).
[3] Su, X. & Norris, A. N., "Focusing, refraction, and asymmetric transmission of elastic waves in solid metamaterials with aligned parallel gaps," Journal of the Acoustical Society of America, 139(6), 3386-3394 (2016).
[4] Su, X., Lu, Z., & Norris, A. N., "Elastic metasurfaces for splitting SV- and P-waves in elastic solids," Journal of Applied Physics, 123(9), 091701 (2018).
[5] Tian, Z., & Yu, L., "Wavefront modulation and controlling for Lamb waves using surface bonded slice lenses," Journal of Applied Physics, 122(23), 234902 (2017).
[6] Tian, Z., & Yu, L., "Elastic phased diffraction gratings for manipulation of ultrasonic guided waves in solids," Physical Review Applied, 11(2), 024052 (2019).
[7] Atli, & K., C., "The effect of tensile deformation on the damping capacity of NiTi shape memory alloy," Journal of Alloys & Compounds, 679, 260-267 (2016).
[8] Mohd Jani, J., Leary, M., Subic, A., & Gibson, M. A., "A review of shape memory alloy research, applications and opportunities," Materials & Design, 56, 1078-1113 (2014)
[9] Ruzzene, M., & Baz, A., "Control of wave propagation in periodic composite rods using shape memory inserts," Journal of Vibration & Acoustics, 122(2), 151-159 (2000)
[10] Ruzzene, M., & Baz, A. M., "Attenuation and localization of wave propagation in periodic rods using shape memory inserts," Smart Materials and Structures, 9(6), 805 (2000).
[11] De Sousa, V. C., Tan, D., Carlos, D. M. J., & Erturk, A., "Tunable metamaterial beam with shape memory alloy resonators: theory and experiment," Applied Physics Letters, 113(14), 143502 (2018).
[12] Chuang, K. C., Lv, X. F., & Wang, D. F., "A tunable elastic metamaterial beam with flat-curved shape memory alloy resonators," Applied Physics Letters, 114(5), 051903 (2019)
[13] Chuang, K. C., Lv, X. F., & Wang, Y. H., "A bandgap switchable elastic metamaterial using shape memory alloys," Journal of Applied Physics, 125(5), 055101 (2019).
[14] Vu, A. H., Hwang, Y. I., Kim, H. J., & Song, S. J., "Focusing ultrasonic wave using metamaterial-based device with cross shape," Journal of the Korean Physical Society, 74(3), 274-279 (2019)